Preprints (www.preprints.org) | NOT PEER-REVIEWED | Posted: 3 October 2022 doi:10.20944/preprints202210.0006.v1

Article

Phosphonate inhibitors of pyruvate dehydrogenase perturb homeostasis of amino acids and protein succinylation in the brain

Artem V. Artiukhov [1,2], Vasily A. Aleshin [1,2], Irina S. Karlina [3], Alexey V. Kazantsev [1,4], Daria A. Sibiryakina [5], Alexander L. Ksenofontov [1], Nikolay V. Lukashev [4], Anastasia V. Graf [1,5] and Victoria I. Bunik [1,2,6]*

[1] Department of Biokinetics, A. N. Belozersky Institute of Physico-Chemical Biology, Lomonosov Moscow State University, 119234 Moscow, Russia; whitelord32br@gmail.com (A.V.A), aleshin_vasily@mail.ru (V.A.A.), mak@org.chem.msu.ru (A.V.K.), ksenofon@belozersky.msu.ru (A.L.K.), nastjushka@gmail.com (A.V.G.)
[2] Department of Biochemistry, Sechenov University, 105043 Moscow, Russia
[3] Department of Clinical Medicine, Sechenov University, 105043 Moscow, Russia; aniram0107@mail.ru
[4] Faculty of Chemistry, Lomonosov Moscow State University, 119234 Moscow, Russia; nvlukashev@gmail.com
[5] Faculty of Biology, Lomonosov Moscow State University, 119234 Moscow, Russia; sibiryakina99@mail.ru
[6] Faculty of Bioengineering and Bioinformatics, Lomonosov Moscow State University, 119234 Moscow, Russia
* Correspondence: bunik@belozersky.msu.ru; Tel.: +7-(495)-939-4484

Abstract: Mitochondrial pyruvate dehydrogenase complex (PDHC) is essential for the brain glucose and neurotransmitter metabolism, dysregulated in many pathologies. Using specific inhibitors of PDHC *in vivo*, we determine biochemical and physiological responses to PDHC dysfunction. Dose dependence of the responses to membrane-permeable dimethyl acetylphosphonate ($AcPMe_2$) is non-monotonous. Primary decreases in glutathione and its redox potential, methionine and ethanolamine are alleviated with increasing PDHC inhibition, the alleviation accompanied by physiological changes. Comparison of 39 brain biochemical parameters after administration of four phosphinate and phosphonate analogs of pyruvate at a fixed dose of 0.1 mmol/kg reveals no primary, but the secondary changes, such as activation of 2-oxoglutarate dehydrogenase complex (OGDHC) and decreased levels of glutamate, isoleucine and leucine. The accompanying decreases in freezing time are most pronounced after administration of acetylmethylphosphinate and dimethyl acetylphosphonate. The PDHC inhibitors do not significantly change the levels of PDHA1 expression and phosphorylation, sirtuin 3 and total protein acetylation, but increase the total protein succinylation and glutarylation, affecting sirtuin 5 expression. Thus, decreased production of the tricarboxylic acid cycle substrate acetyl-CoA by inhibited PDHC is compensated by increased degradation of amino acids through the cycle with activated OGDHC, increasing total protein succinylation/glutarylation and decreasing anxiety indicators.

Keywords (3-10 words): branched chain 2-oxo acids; 2-oxoglutarate dehydrogenase; pyruvate dehydrogenase; phosphonate and phosphinate analogs of pyruvate; protein succinylation; protein acetylation; protein glutarylation; sirtuin 3; sirtuin 5; anxiety

1. Introduction

The thiamine diphosphate (ThDP)-dependent pyruvate dehydrogenase (PDH, 1.2.4.1) functions within multienzyme pyruvate dehydrogenase complex (PDHC) that links cytosolic glycolysis with mitochondrial tricarboxylic acid (TCA) cycle. Oxidizing the glycolytic product pyruvate, PDHC produces the TCA cycle substrate acetyl-CoA and NADH to be oxidized in the mitochondrial electron transport chain. In addition, the PDHC reactive acetyl intermediates and the product acetyl-CoA donate acetyl moieties for post-translational modifications of proteins, that are of regulatory significance [1-3]. Although there are different sources of acetyl-CoA for the protein acetylation,

© 2022 by the author(s). Distributed under a Creative Commons CC BY license.

Preprints (www.preprints.org) | NOT PEER-REVIEWED | Posted: 3 October 2022 doi:10.20944/preprints202210.0006.v1

participation of PDHC in acetylation of histones is shown [4,5] along with the observations of PDHC [4] and its PDH component [5,6] in cell nucleus. PDHC-dependent acetylation of metabolic proteins has not received significant attention, apart from early studies on autoacetylation of PDHC [1]. The goal of the current work is to reveal the consequences of inhibition of the PDHC reaction on the brain biochemical indicators of the major role of PDHC in mitochondrial metabolism, along with impact of PDHC inhibition on physiological state of the animals.

Different pharmacological tools are available for PDHC regulation. Thiamine (vitamin B1) and its pharmacological forms are precursors for a PDHC coenzyme, ThDP [7,8]. In addition to the thiamine-related activators of PDHC reaction, antagonists of thiamine [7-9] and of another coenzyme of PDHC, covalently bound lipoic acid [10-12], may be used to inhibit the reaction. However, these compounds would affect all the complexes of dehydrogenases of 2-oxo acids. In contrast, inhibition of PDHC by synthetic analogs of pyruvate is an effective way to target specifically PDHC, not affecting the other family members [9,13,14]. Hence, in this work we apply the phosphonate inhibitors of PDH to reveal the consequences of the brain PDHC dysfunction for the biochemical and physiological parameters. Using the membrane penetrating dimethyl ester of acetyl phosphonate ($AcPMe_2$), we characterize the dose dependence of the changes. Furthermore, we use a fixed dose of the different phosphonate analogs of pyruvate, shown in Figure 1, to characterize their relative efficacy *in vivo*.

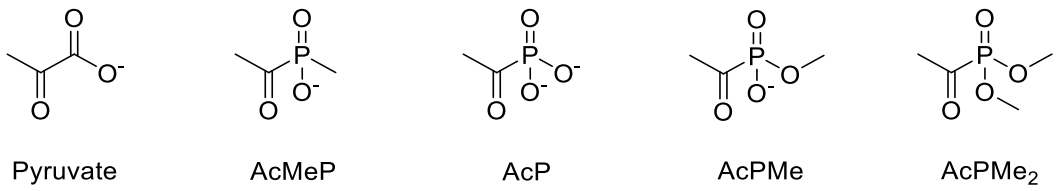

Figure 1. Structures of pyruvate and its phosphinate and phosphonate analogs, used in this study. Phosphinate analogs of pyruvate include acetylmethylphosphinate (AcMeP). Phosphonate analogs of pyruvate include acetyl phosphonate (AcP) and its methyl (AcPMe) and dimethyl esters ($AcPMe_2$).

2. Results

2.1. Dose-dependent effects of dimethyl ester of acetyl phosphonate on metabolism and physiology.

The fully esterified phosphonate $AcPMe_2$ (Figure 1) is known to cause a strong viability decrease upon its incubation with cell cultures [14,15]. No charged groups allow $AcPMe_2$ to diffuse through biological membranes, whereas the charged analogs require protein transporters/channels to penetrate the membrane. As a result, compared to $AcPMe_2$, intracellular concentration of the charged analogs is expected to be a more complex function of their extracellular concentration and intracellular transport. Hence, $AcPMe_2$ has been chosen to study the concentration dependence of inhibition of the brain PDHC *in vivo*. The metabolic indicators of PDHC function in the TCA cycle, used to characterise the action of PDHC inhibitors, are shown in Figure 2. Apart from the PDHC activity, important enzymatic indicators of the PDHC-dependent flux through the TCA cycle are employed. They are represented by the activities of (i) the TCA-cycle-limiting 2-oxoglutarate dehydrogenase complex (OGDHC), (ii) the enzymes metabolising malate, i.e. malate dehydrogenase (MDH) and decarboxylating malic enzyme (ME) important for anaplerosis, and (iii) glutamine synthetase (GS) whose function is linked to the amino acid degradation occurring in the TCA cycle [16]. Accordingly, the profile of the brain amino acids and related compounds is a useful indicator of the TCA cycle substrate fluxes [16,17].

Preprints (www.preprints.org) | NOT PEER-REVIEWED | Posted: 3 October 2022 doi:10.20944/preprints202210.0006.v1

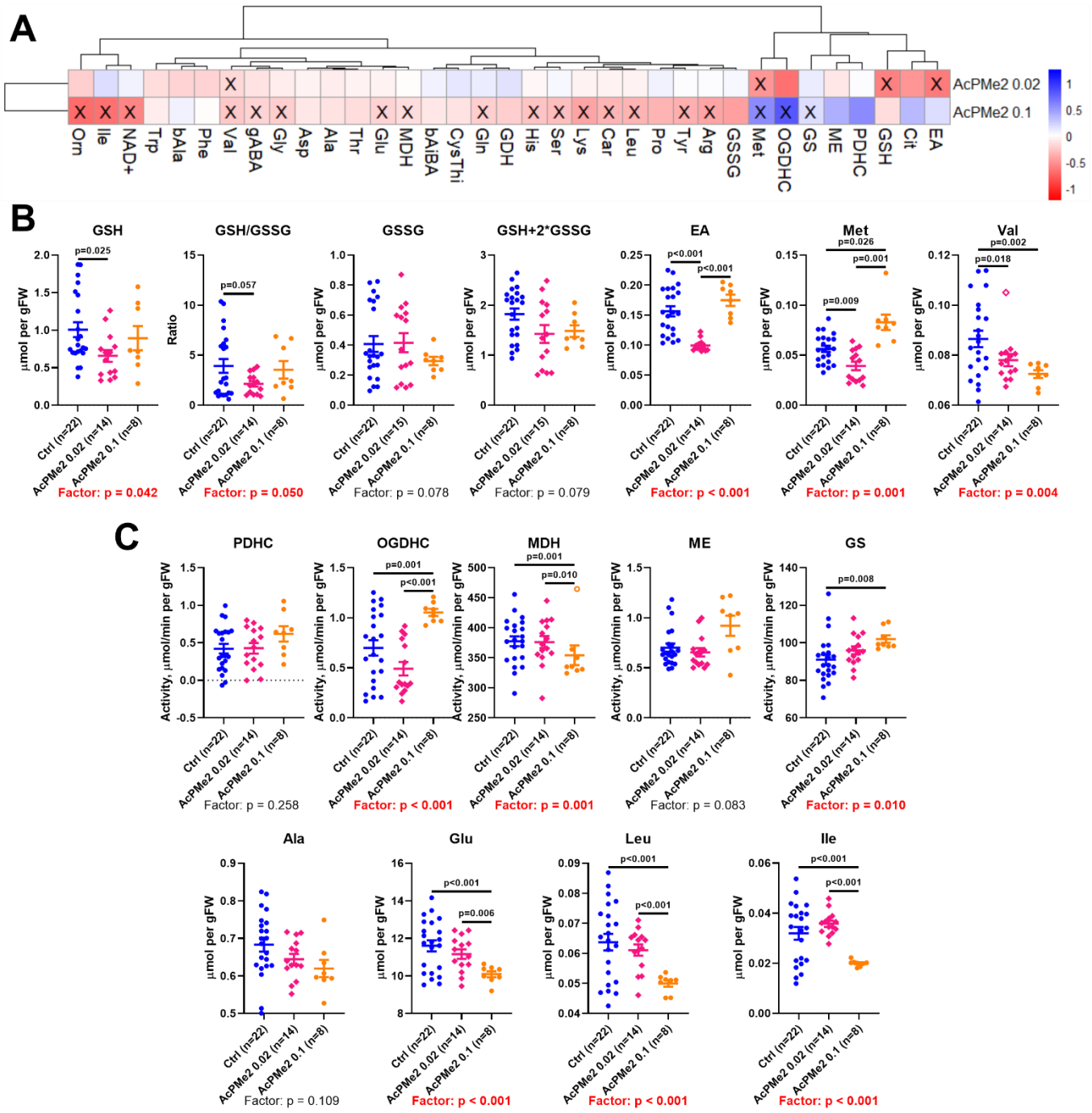

Figure 2. Dose-dependent effects of dimethyl ester of acetyl phosphonate ($AcPMe_2$) on biochemical parameters of the rat cerebral cortex. (A) $AcPMe_2$-induced changes in the levels of metabolites and enzymatic activities are presented as log2 of the fold change from the non-treated animals. (B) Significant changes in the levels of amino acids and related compounds upon treatment with low dosage (0.02 mmol/kg) of $AcPMe_2$. (C) Significant changes in the enzyme activities and levels of amino acids upon treatment with high dosage (0.1 mmol/kg) of $AcPMe_2$. Enzyme activities are presented as µmol/min per gram of tissue fresh weight (gFW), levels of metabolites – as µmol per gFW. Significant ($p \leq 0.05$) differences between experimental groups, estimated by ANOVA with Tukey's post-hoc test, are indicated as crossed cells on the heatmap (A; $p \leq 0.05$ *vs* Ctrl) or as exact *p*-values on the graphs (B, C). The ANOVA *p*-values for the treatment factor significance are shown below the graphs, with significant values of $p \leq 0.05$ marked in red. Empty symbols denote outliers determined by the iterative Grubb's test. Number of the animals in the groups and dosages of the administered $AcPMe_2$ are indicated on X axes. Proteinogenic amino acids are abbreviated according to the standard 3-letter code. Other abbreviations used are: Cntr – control, bAiBA—β-aminoisobutyrate, bAla—β-alanine, Car—carnosine, CysThi—cystathionine, EA—ethanolamine, gABA—γ-

Preprints (www.preprints.org) | NOT PEER-REVIEWED | Posted: 3 October 2022 doi:10.20944/preprints202210.0006.v1

aminobutyrate, GSH – reduced glutathione, GSSG – oxidized glutathione, Orn—ornithine, GDH—glutamate dehydrogenase, MDH— malate dehydrogenase, ME — $NADP^+$-dependent malic enzyme. GS — glutamine synthetase.

In accordance with the reversibility of the phosphonate inhibitors binding to PDHC [9], no alterations in the activity of PDHC assayed upon a strong dilution of the brain homogenates in the reaction medium, is observed (Figure 2). However, dose-dependent changes in many metabolic indicators (Figure 2A) point to strong perturbation of brain metabolism upon the PDHC inhibition *in vivo*.

At the low $AcPMe_2$ dose (0.02 mmol/kg), significant decreases in glutathione and its redox potential, ethanolamine, methionine and valine are observed (Figures 2A, 2B). Thus, these changes are primary indicators of the PDHC impairment. Upon the administration of a high $AcPMe_2$ dosage (0.1 mmol/kg), decreases in these primary indicators, except for that of valine, are alleviated (Figure 2B). The switch is accompanied by changes in the activities of OGDHC, MDH and GS (Figure 2C). Remarkably, activities of PDHC and the pyruvate-producing malic enzyme (ME), along with a known indicator of the pyruvate oxidation in the TCA cycle, alanine, do not significantly change. The finding suggests homeostatic stabilization of the pyruvate/alanine ratio at the metabolite level through the network of transamination reactions. In contrast, activity of malate dehydrogenase (MDH) producing oxalacetate for condensation with acetyl-CoA, is decreased (Figure 2C). The decrease is in accord with an inhibited acetyl-CoA flux into TCA cycle. At the same time, activity of OGDHC increases in response to the high level of PDHC inhibition *in vivo*, along with a decrease in the brain level of glutamate. Not only the activated OGDHC promotes glutamate oxidation in the TCA cycle, but also the glutamate usage for biosynthesis obviously contributes to the decrease in glutamate levels. Indeed, at the high $AcPMe_2$ dose the glutathione level returns to the control one (Figure 2B), and production of glutamine from glutamate by glutamine synthetase (GS) is activated (Figure 2C). The increased activity of GS indicates increased ammoniac production due to the degradation of amino acids in the TCA cycle with activated OGDHC. Indeed, at the strong PDHC inhibition *in vivo*, the branched-chain amino acids leucine and isoleucine decrease (Figure 2C), in addition to the primarily decreased valine (Figure 2B).

The high dose of $AcPMe_2$ also affects the physiological state: RMSSD of ECG decreases along with an increase in the locomotor activity, estimated by crossing the lines in the Open Field Test (Figure 3). Biphasic response of physiological parameters to increasing dose of the PDHC inhibitor is evident from significant differences between the effects of the two different doses of $AcPMe_2$, although the low dose shows no effect *vs* control animals. This is manifested in the line crossing and freezing time (Figure 3), pointing to the opposite changes in these parameters at the two doses of the inhibitor. Thus, the physiological effects of PDHC inhibition show a complex dependence on the inhibitor dosage, similar to the brain biochemical parameters.

Preprints (www.preprints.org) | NOT PEER-REVIEWED | Posted: 3 October 2022 doi:10.20944/preprints202210.0006.v1

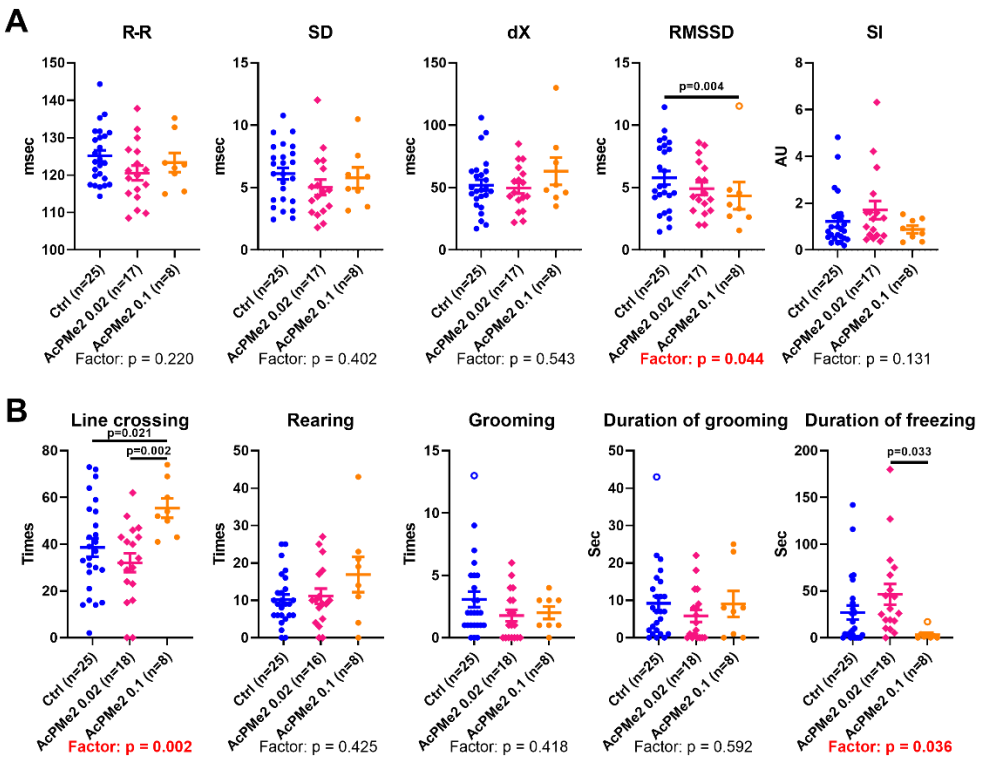

Figure 3. Changes in animal physiology after administration of the indicated dosages of AcPMe2. (A) Heart variability parameters obtained from ECG. (B) Behavioural parameters obtained in the Open Field Test. Significant differences of the treatments and between experimental groups are estimated and shown in the same way as in Figure 2.

2.2. Comparison of the biochemical and physiological effects of the phosphinate and phosphonate inhibitors of PDHC.

The biochemical and physiological effects of the phosphinate (AcMeP) and phosphonate (AcP, AcPMe, AcPMe2) analogs of pyruvate (Figure 1), known to be of different inhibition power from *in vitro* studies [9,14,18], have been compared after administration to animals of the same dosage of the drugs (0.1 mmol/kg). *In vitro*, the inhibitory power of the charged analogs decreases in the order AcMeP < AcP < AcPMe, but inside the cells cellular esterases may de-esterify both the mono- (AcPMe) and dimethyl (AcPMe2) esters to AcP. These considerations are in accord with the automatically obtained clusters of the inhibitors-induced changes in the brain biochemical parameters, shown in Figure 4A. That is, the clusters shown at the left of Figure 4A, indicate that the changes induced by the strongest *in vitro* phosphinate inhibitor AcMeP are separated from the changes induced by the phosphonate inhibitors AcP, AcPMe and AcPMe2, with the latter three forming a common cluster.

Furthermore, none of the inhibitors significantly affect the assayed levels of PDHC activity and alanine, but all the inhibitors increase activity of OGDHC, decreasing the levels of glutamate and branched-chain amino acids, with NAD^+ mostly decreased as well (Figure 4B). Although MDH is decreased by AcPMe2 only, the primary changes, occurring at the low dose of AcPMe2, i.e. the decreases in the level and redox potential of glutathione or in the levels of ethanolamine and methionine (Figure 2B), are not observed for any of the analogs (Figure 4C). As a result, the most essential changes observed after administration of the fixed dose of all the analogs (Figure 4B, 4C), are similar to those after administration of the high dose of AcPMe2 (Figure 2). Thus, administration of all the employed analogs results in the PDHC inhibition level that corresponds to the second phase of the induced changes.

Preprints (www.preprints.org) | NOT PEER-REVIEWED | Posted: 3 October 2022 doi:10.20944/preprints202210.0006.v1

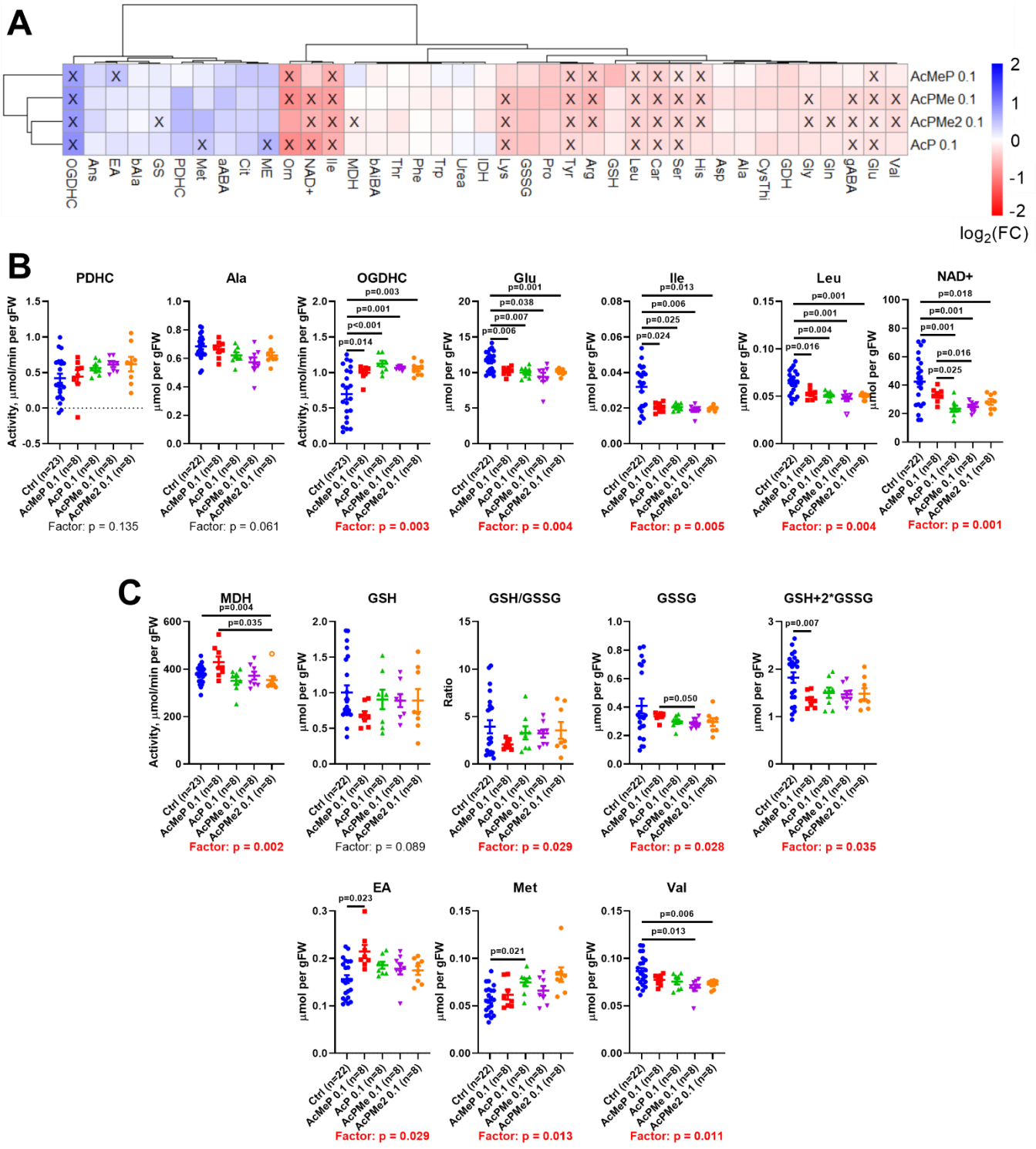

Figure 4. Comparison of the actions of the phosphinate and phosphonate analogs of pyruvate on the biochemical parameters of the rat cerebral cortex. (A) Levels of metabolites and enzymatic activities are presented as log2 of the fold change in the treated *vs* untreated animals. (B) Activities of PDHC and associated enzymes. (C) Changes in MDH and primary indicators of PDHC function. Significant differences between experimental groups are estimated and shown in the same way as in Figure 2. Abbreviations are the same as in Figure 2. Other abbreviations: aABA – α-aminobutyrate, Ans – anserine, IDH – $NADP^+$-dependent isocitrate dehydrogenase.

The high inhibition level by all the analogs is further supported by physiological changes. The treatment factor is of significance for RMSSD of ECG (p=0.041) and duration

Preprints (www.preprints.org) | NOT PEER-REVIEWED | Posted: 3 October 2022 doi:10.20944/preprints202210.0006.v1

of freezing (p=0.012). Both decrease after administration of PDHC inhibition, with the most significant decreases *vs* control animals observed after administration of the strongest *in vitro* inhibitor AcMeP and/or membrane-penetrating $AcPMe_2$ (Figure 5).

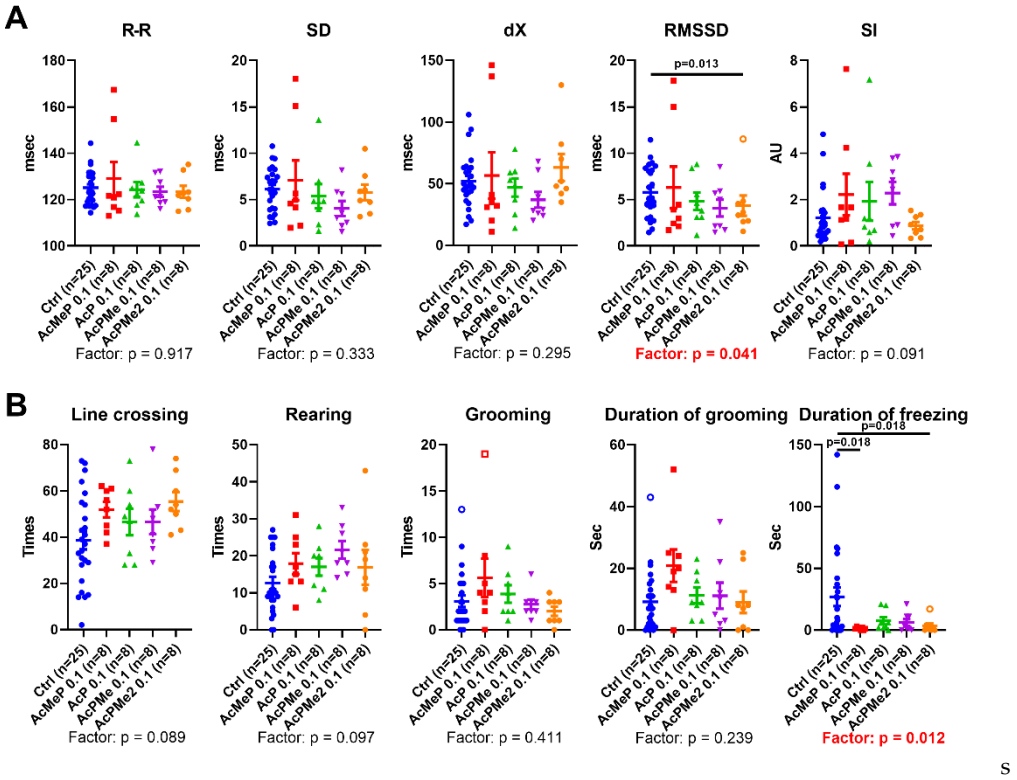

Figure 5. Effects of phosphonate and phosphinate analogs of pyruvate on the animal physiology. (A) Heart variability parameters obtained from ECG. (B) Behavioural parameters obtained in the Open Field Test. Significant differences of the treatments and between experimental groups are estimated and shown in the same way as in Figure 2.

2.3. Action of the PDHC inhibitors on the PDHA expressioin and its active site phosphorylation at Ser293

In view of the regulation of the PDHC activity by phosphorylation of its rate-determining component at the active site residue Ser293 of PDHA1 subunit, we assessed the action of the PDHC inhibitors on the enzyme expression and phosphorylation. After the administration of the inhibitors at 0.1 mmol/kg, no significant changes are observed in either the PDHA1 expression (Figure 6A) or its phosphorylation at Ser293 (Figure 6B). Moreover, the phosphorylation normalized to the expression level, does not change either (Figure 6C).

Preprints (www.preprints.org) | NOT PEER-REVIEWED | Posted: 3 October 2022 doi:10.20944/preprints202210.0006.v1

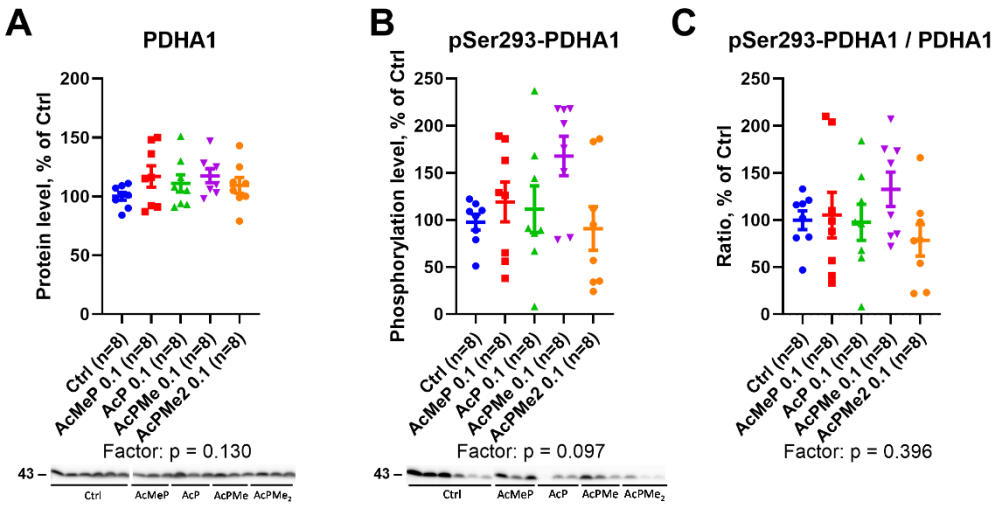

Figure 6. Expression and phosphorylation of PDHA1 subunit after the action of the PDHC inhibitors administered at 0.1 mmol/kg. A – Protein levels of PDHA1. B – Levels of PDHA1 phosphorylation at Ser293 residue. C – Levels of PDHA1 phosphorylation, normalized to the protein expression in the same samples. Data are presented as % from the indicated parameters in the control (Ctrl) animals. Significance of the treatment factors and differences between experimental groups are estimated and shown in the same way as in Figure 2.

2.4. Changes in total levels of the brain protein acylations induced by the PDHC inhibitors.

Changes in acylations of the brain proteins and expression of deacylases sirtuins 3 and 5 upon inhibition of the acetyl-CoA production by PDHC are shown in Figure 7. The levels of total protein acetylation and mitochondrial deacetylase sirtuin 3 are not significantly changed (Figure 7A, 7B). However, the PDHC inhibition induces significant changes in the system of the negatively charged acylations: Levels of total succinylation and glutarylation of the brain proteins are increased, while expression of the corresponding deacylase sirtuin 5 is down-regulated (Figure 7C-E).

Correlation analysis of the brain components of the acylation system in the pooled sample of studied animals (Figure 8) points to significant negative correlations of the levels of total succinylation with NAD^+ and of the levels of total glutarylation with sirtuin 3. Besides, sirtuin 3 is positively correlated with total acetylation of the brain proteins, while sirtuin 5 is correlated negatively with the OGDHC activity and positively with NAD^+ levels. Remarkably, the phosphorylation of PDHA1 subunit of PDHC positively correlates with the level of total succinylation of the brain proteins. This correlation complements the finding that PDHC inhibition increases total succinylation (Figure 7C), as also PDHA1 phosphorylation decreases the PDHC activity. Thus, across the studied conditions, the brain protein succinylation increases with increasing inactivation of PDHC by its phosphorylation or inhibition and decreasing the desuccinylase substrate NAD^+. In contrast, total acetylation of the brain proteins has an intrinsic adjustment mechanism, increasing expression of sirtuin 3 along with increased protein acetylation. Finally, our data show different regulatory networks for the succinylation and glutarylation of the brain proteins. On one hand, levels of both types of the acylation increase upon the PDHC inhibition simultaneously with down-regulation in sirtuin 5 (Figure 7) and up-regulation of the OGDHC activity (Figure 4), that are negatively correlated (Figure 8). On the other hand, the correlation analysis indicates that under the same set of conditions, the succinylation and glutarylation show different interdependences on the factors essential for the acylation levels (Figure 8). The succinylation is strongly linked to the availability of the desuccinylase substrate NAD^+, whose decrease expectedly increases the succinylation. In contrast, the glutarylation shows a more complex control, being strongly linked to the acetylation system. That is, the glutarylation decreases along with increasing expression of the deacetylase sirtuin 3.

Preprints (www.preprints.org) | NOT PEER-REVIEWED | Posted: 3 October 2022 doi:10.20944/preprints202210.0006.v1

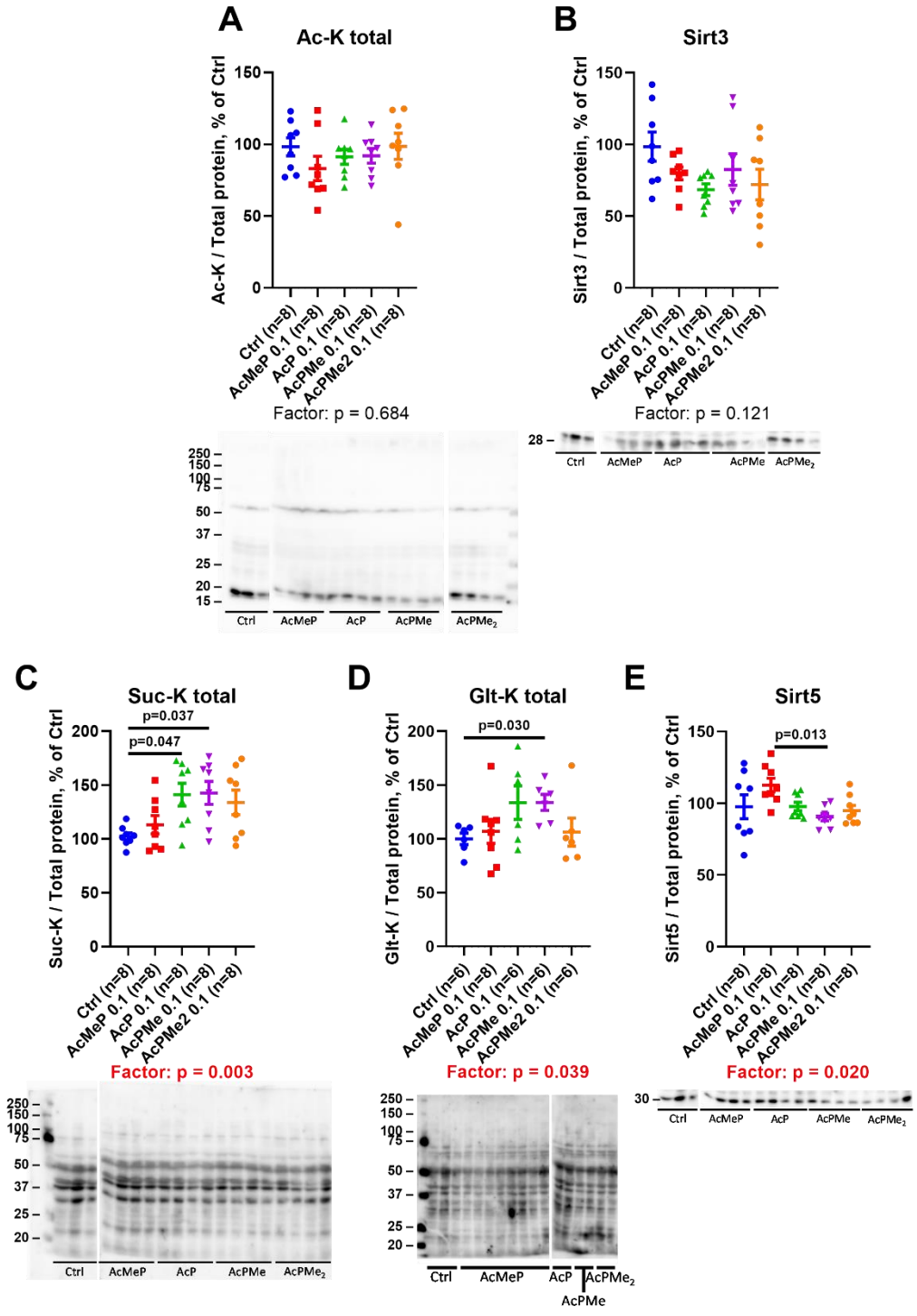

Figure 7. Changes in the components of acylation system in the cerebral cortex upon the administration of PDHC inhibitors. (A) Total protein acetylation (Ac-K). (B) Sirtuin 3 expression. (C) Total protein succinylation (Suc-K). (D) Total protein glutarylation (Glt-K). (E) Sirtuin 5 expression. Protein expression and acylation are determined by immunoblottings, shown below the graphs. Data are presented as % from the non-treated animals. Significant differences of the treatments and between experimental groups are estimated and shown in the same way as in Figure 2.

Preprints (www.preprints.org) | NOT PEER-REVIEWED | Posted: 3 October 2022 doi:10.20944/preprints202210.0006.v1

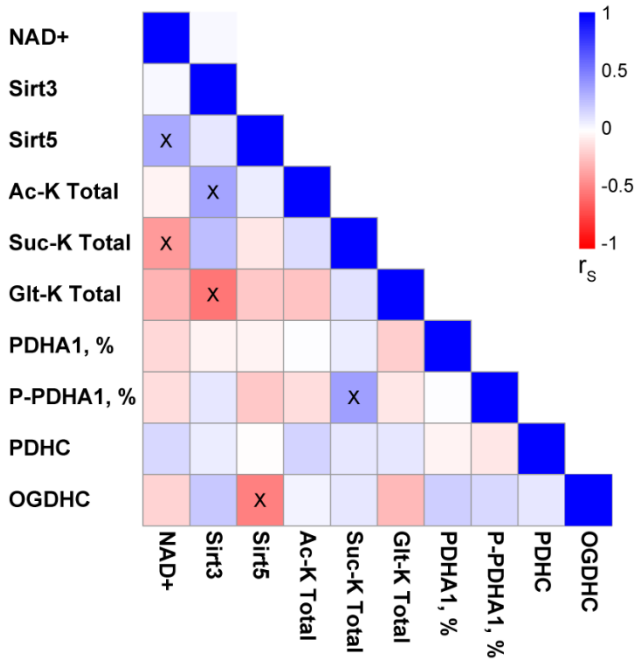

Figure 8. Pairwise correlations between the components of the brain acylation system. Spearman correlation coefficients (rs) and the significances of the correlations (crossed cells correspond to $p < 0.05$) are calculated for the indicated pairs of the parameters using the pooled sample of studied animals (n=40).

3. Discussion

The dose dependence of the brain biochemical response to the PDHC inhibition, shown in this study, demonstrates biphasic changes in the brain metabolism with increasing PDHC inhibition. In view of the recently shown biphasic response of the brain metabolism to inhibition of OGDHC [19], we conclude that the biphasicity is an essential feature of the perturbation in these critical branch points of animal metabolism, interconnected through the TCA cycle. In both cases, the primary changes in the levels of critical metabolites induce a homeostatic response that is directed to alleviation of such changes. However, this process brings about secondary changes in other parts of the perturbed metabolic network.

The primary changes upon the PDHC inhibition (Figure 2B) affect the metabolites essential for the glutathione redox-state (glutathione), phospholipid biosynthesis (ethanolamine) [20,21], or anabolic reactions requiring adenosyl methionine (methionine). Remarkably, dihydrolipoic acid, an intermediate of the PDHC reaction, reduces peroxidized phospholipids, including oxygenated phosphatidylethanolamine [22]. One of the most abundant mammalian phospholipids, phosphatidylethanolamine is known to participate in autophagy, ferroptosis, endoplasmic reticulum stress and Parkinson's disease [21,22]. Phosphatidylethanolamine alleviates mitochondrial dysfunction induced by insufficiency of the mitochondria-specific phospholipid cardiolipin [23] which activates PDHC [24]. Translocation of cardiolipin from the inner to outer mitochondrial membrane, known to induce mitophagy [25], may thus bring about deactivation of the cardiolipin-activated PDHC, similar to the PDHC activity loss due to inhibition. In view of these independent data on functional interactions between PDHC, the phospholipids and mitochondrial dysfunction, our finding that the PDHC inhibition in the brain causes biphasic changes in the brain level of ethanolamine (Figure 2) indicates increased synthesis of phosphatidylethanolamine from ethanolamine as a primary response to PDHC inhibition. Remarkably, biosynthesis of phosphatidylethanolamine occurs from either ethanolamine or serine [23]. The secondary decrease in the brain serine levels is a universal consequence of the action of all PDHC inhibitors at the high dose (Figure 4A). The finding suggests an increase in the phosphatidylethanolamine formation from serine, compensating for the primary decrease in ethanolamine content at the low dose of PDHC inhibition (Figure 2B). The

Preprints (www.preprints.org) | NOT PEER-REVIEWED | Posted: 3 October 2022 doi:10.20944/preprints202210.0006.v1

inhibition-induced switch to another biosynthetic pathway may contribute to the normalization of ethanolamine level observed after the primary decrease (Figure 2B).

Up-regulation of the TCA-cycle-limiting OGDHC and increased amino acids degradation through the cycle compensate for the mitochondrial energy production at the perturbed entry of acetyl-CoA into the cycle. Remarkably, both the OGDHC and PDHC inhibition induce increases in the OGDHC activity and biphasic changes in the glutathione metabolism. However, when OGDHC is inhibited, the OGDHC activity increase is a primary response, followed by the activity decrease. Accordingly, administration of both the OGDHC and PDHC inhibitors affects the brain glutathione metabolism, yet the primary effect of the OGDHC inhibition is manifested in the glutathione disulfide levels [19], while that of the PDHC inhibition – in the levels of reduced glutathione (Figure 2). Inhibition of both the complexes changes the physiological parameters along with the secondary changes in the brain biochemistry, affecting indicators of anxiety and stress.

Compensatory response to the PDHC inhibition could include the dephosphorylation of the first component of the complex to increase PDHC activity. However, this does not occur, at least under the induced levels of the enzyme inhibition (Figure 6). The total acetylation of the brain proteins does not change either, in contrast to succinylation and glutarylation, dependent on the function of OGDHC or its second and third components, which are common for OGDHC and the analogous 2-oxoadipate dehydrogenase complex (OADHC) (Figure 7A). Thus, the total acylation of the brain proteins is in accord with the changed activity of OGDHC and no changes in that of PDHC (Figure 2, 4). Nevertheless, the level of PDHA1 phosphorylation shows a strong positive correlation with the total succinylation (Figure 8), revealing interconnected regulation of the two post-translational modifications of the brain proteins. The lower the PDHC activity due to the PDHA1 phosphorylation, the higher the protein succinylation level. This result of the correlation analysis is supported by the same action on the succinylation of the PDHC inhibitors (Figure 7C) and PDHC inactivation by phosphorylation (Figure 8). Probably, the relationship manifests the competition between the parallel reactions of succinylation and acetylation of the protein lysine residues. Besides, the total succinylation increases along with the increase of the OGDHC activity (Figure 4B) that is also negatively correlated to the desuccinylase sirtuin 5 (Figure 8). Finally, total succinylation correlates negatively with the levels of the deacylases substrate NAD^+. As a result, under the studied conditions of the PDHC inhibition, the levels of the OGDHC activity, PDHA1 phosphorylation and NAD^+ contribute the most to the protein succinylation.

Reduced acetyl-CoA production by PDHC is known to decrease biosynthesis of acetylcholine in the brain or neurons [26,27]. This is observed in the thiamine deficiency states [28-32], exposures to β-amyloid [33], aluminium, zinc ions or nitric oxide [31,32,34]. The observed decreases in RMSSD and duration of freezing (Figures 3, 5) are in accordance with the PDHC-inhibition-induced decrease in the brain acetylcholine, shown in the independent studies mentioned above.

Thus, the characterized metabolic action of specific inhibitors of PDHC unravels molecular mechanisms involved in the brain homeostatic response to perturbed PDHC function, the secondary metabolic perturbations and their physiological impact.

4. Materials and Methods.

4.1. Reagents

Sodium salt of AcMeP was synthesized according to [18,35]. Methyldichlorophosphine (0.1 mol, 11.69 g, 8.84 ml) was added to trimethyl orthoacetate (0.228 mol, 27.35 g, 29 ml) at -30°C. The resulting mixture was stirred at ambient temperature for 18 h. The excess of trimethyl orthoacetate was removed under reduced pressure The product (methyl (1,1-dimethoxyethyl)methylphosphinate) was isolated by vacuum distillation. Yield: 15.1 g (83%), b.p. 81-83°C/0.9 mm. NMR ^{1}H ($CDCl_3$), δ, ppm: 3.76 (d, *J* 10.2 Hz, 3H, $(CH_3O)P(O)$), 3.37 (d, *J* 6.6 Hz, 6H, $C(OCH_3)_2$), 1.46 (d, *J* 2.3 Hz, 3H, CH_3C), 1.42 (s, 3H, CH_3P). NMR ^{13}C ($CDCl_3$), δ, ppm: 100.7 (d, *J* 143.3 Hz, $\underline{C}CH_3$), 51.7 (d, *J* 6.7 Hz,

Preprints (www.preprints.org) | NOT PEER-REVIEWED | Posted: 3 October 2022 doi:10.20944/preprints202210.0006.v1

(CH_3O)P(O)), 49.8 (d, *J* 5.9 Hz, C(O$\underline{C}H_3)_2$), 49.6 (d, *J* 6.7 Hz, C(O$\underline{C}H_3)_2$), 19.0 (d, *J* 12.7 Hz, C$\underline{C}H_3$), 10.7 (d, *J* 89.4 Hz, CH_3P). NMR ^{31}P ($CDCl_3$), δ, ppm: 49.5.

To obtain sodium (1,1-dimethoxyethyl)methylphosphinate, a solution of methyl (1,1-dimethoxyethyl)methylphosphinate (10 mmol, 1.82 g) and NaI (11 mmol, 1.65 mg) in 11.4 ml of dry methylethylketone was refluxed for 2 h under argon. The resulting precipitate was filtered off, washed twice with 5 ml of dry acetone and dried in vacuo. Yield: 1.56 g (82.2%), m.p. 186-188°C. NMR ^{1}H (D_2O), δ, ppm: 3.36 (s, 6H, C($OCH_3)_2$), 1.43 (d, *J* 10.1 Hz, 3H, CH_3C), 1.27 (d, *J* 13.4 Hz, 3H, CH_3P). NMR ^{13}C (D_2O), δ, ppm: 101.4 (d, *J* 141.6 Hz, $\underline{C}CH_3$), 49.8 (d, *J* 5.9 Hz, C(O$\underline{C}H_3)_2$) 18.4 (d, *J* 11.0 Hz, C$\underline{C}H_3$), 13.3 (d, *J* 89.4 Hz, CH_3P). NMR ^{31}P (D_2O), δ, ppm: 37.5.

Sodium (1,1-dimethoxyethyl)methylphosphinate (5.9 mmol, 1.12 g) was further dissolved in a mixture of 5.9 ml of glacial acetic acid and 0.35 ml of water. The solution was stirred at ambient temperature for 24 h. The solvent was evaporated to dryness and residue was triturated with 30 ml of acetone and filtered off to give sodium AcMeP as white solid. Yield: 0.8 g (94.3%), m.p. 195-197°C. NMR ^{1}H (D_2O), δ, ppm: 2.42 (d, *J* 3.8 Hz, 3H, CH_3C(O)), 1.36 (d, *J* 14.2 Hz, 3H, CH_3P). NMR ^{13}C (D_2O), δ, ppm: 224.5 (d, *J* 109.6 Hz, C(O)P(O)), 27.9 (d, *J* 42.2 Hz, $\underline{C}H_3$C(O)), 12.3 (d, *J* 95.3 Hz, CH_3P). NMR ^{31}P (D_2O), δ, ppm: 27.1.

$AcPMe_2$ was synthesized from dimethyl phosphite and acetyl chloride as described previously [14]. Partial hydrolysis of $AcPMe_2$ with NaI according to [14] resulted in sodium salt of AcPMe. Complete hydrolysis with $NaHCO_3$ resulting in disodium salt of AcP, was done according to [36]. Bromotrimethylsylane (40 mmol, 6.12 g, 5.3 ml) was added dropwise to $AcPMe_2$ (10 mmol, 1.52 g) stirred at 0°C under argon. The resultant solution was stirred at ambient temperature overnight. The excess of bromotrimethylsilane was removed under reduced pressure. Aqueous $NaHCO_3$ (1M, 20 ml) was added at 0°C and the solution stirred at 0°C for 1 h. Water was evaporated to dryness under reduced pressure and residue was washed with 10 ml of absolute ethanol to give the product as white solid. Yield: 1.56 g (93%). NMR ^{1}H (D_2O), δ, ppm: 2.34 d (3H, C(O)CH_3, *J* 3.6 Hz). NMR ^{13}C (D_2O), δ, ppm: 29.8 (d, *J* 43.7 Hz, C(O)$\underline{C}H_3$), 228.2 (d, *J* 157.0 Hz, $\underline{C}$(O)CH_3). NMR ^{31}P (D_2O), δ, ppm: -0.1.

NAD^+ was obtained from Gerbu (Heidelberg, Germany), oxidized glutathione—from Calbiochem (La Jolla, CA, USA). Formate dehydrogenase for NAD^+ assays was obtained from the Federal Research Center of Biotechnology/Innotech MSU (Moscow, Russia). All other reagents were of the highest purity available and obtained from Sigma-Aldrich (Helicon, Moscow, Russia).

4.2. Animal Experiments

Animal experiments were performed according to the Guide for the Care and Use of Laboratory Animals published by the European Union Directives 86/609/EEC and 2010/63/EU, and were approved by the Bioethics Committee of Lomonosov Moscow State University (protocols number 69-o from 09.06.2016 and 139-a from 11.11.2021). Wistar male rats were kept in standard conditions with 12 h light and 12 h dark day cycle, with free access to water and food. Phosphinate and phosphonate analogs of pyruvate were dissolved in deionized water to obtain 0.2 M or 1 M solutions and administered intranasally at 0.02 mmol/kg ($AcPMe_2$, only) or 0.1 mmol/kg dosage (all phosphonates), respectively. Physiological solution (0.9% NaCl) was administered to the control animal group. 24 h after the administration, the rats were subjected to physiological tests and sacrificed by decapitation as described before [37,38]. Immediately after the decapitation, the animal brain was excised and the brain cortex was separated on ice and frozen in liquid nitrogen within 90 s after decapitation. The tissue samples were stored at −70°C until the biochemical assays.

4.3. Physiological Tests

Estimation of behavioral activity was performed using "Open Field" test as described previously [37,39]. ECG was recorded using for 3 min using non-invasive electrode placement [37]. The heart rate variability parameters calculated from ECG recordings are described previously [37].

Preprints (www.preprints.org) | NOT PEER-REVIEWED | Posted: 3 October 2022 doi:10.20944/preprints202210.0006.v1

4.4. Metabolite and Enzyme Activity Assays

Quantification of low-molecular weight metabolites was done in methanol/acetic acid extracts of rat cerebral cortex prepared according to previously published research [40]. Amino acids and other amino compounds were quantified using cation-exchange chromatography with post-column ninhydrin derivatization [40]. Quantitave determination of other metabolites, including NAD^+ and oxidized glutathione, was performed according to published protocols as described elsewhere [19]. The levels of all metabolites were calculated in μmoles per gram of tissue fresh weight (gFW).

Enzyme activities were measured in cerebral cortex homogenates prepared as described previously [16,19,41]. Spectrophotometric assays for glutamate dehydrogenase, malate dehydrogenase, $NADP^+$-dependent malic enzyme, glutamine synthetase, PDHC and OGDHC are described in previous papers [16,19,41]. For OGDHC assay the blank media did not contain coenzyme A. $NADP^+$-dependent isocitrate dehydrogenase was assayed in previously described medium [41]. The reaction was started with addition of 3 μL of homogenate and monitored for 10 min. The resulting reaction slope was corrected for blank reaction assayed without D,L-isocitrate. The assayed enzyme activities were expressed as μmoles of substrate consumed or product generated per minute per gFW.

4.5. Western blotting

The tissue homogenates were diluted in Laemmli buffer and subjected to SDS-PAGE as described previously [38]. The levels of total protein succinylation and glutarylation were estimated by western-blotting using primary antibodies #PTM-401 and #PTM-1151, respectively, from PTM Biolabs (Chicago, IL, United States). The levels of total protein acetylation, sirtuin 3, sirtuin 5, PDHA1 and phosphorylated PDHA1 were estimated using antibodies #9841, #5490, #8782, #3205 and #37115, respectively, from Cell Signaling Technology (Danvers, MA, USA). All primary antibodies were used in 1:2000 dilution. Secondary HRP-conjugated anti-rabbit antibody from Cell Signaling Technology, #7074 (Danvers, Massachusetts, USA) was used in 1:3000 dilution. Relative chemiluminescence was detected using ChemiDoc MP Imager (Bio-Rad, Hercules, CA, USA) and processed in Image Lab software v. 6.0.1 (Bio-Rad, Hercules, CA, USA). Normalization was done per total protein level in gel lane, determined via 2,2,2-tricholoroethanol staining as described elsewhere [42]. When comparing several membranes, the band intensities from different membranes were further normalized to the levels in common samples present in all the membranes. Raw images of membranes with visualized protein bands are presented in Supplementary Figure S1.

4.6. Statistics and Data Analysis

Data are presented as mean ± standard error of the mean for each experimental group. Due to noticeable differences in the variances of the parameters in the experimental groups, the latter were compared using one-way Welch ANOVA with recommended Games-Howell's *post hoc* test, employed in GraphPad Prism 9.0 (GraphPad Software Inc., La Jolla, USA) or *userfriendlyscience* package in R. The differences with $p \leq 0.05$ were considered significant. Outliers (indicated as hollow points in graphs) were identified according to the iterative Grubb's test (alpha = 0.01) in each experimental group and excluded from statistical analysis. The number of animals in experimental groups (n) is indicated including outliers.

According to the Shapiro-Wilk test, some of the biochemical parameters were not normally distributed. Thus, for analysis of the components of protein acylation system, Spearman's correlation coefficients were calculated for each pair of the parameters. Heatmaps including correlation matrices were prepared using RStudio 1.4 (Rstudio, PBC, Boston, MA, USA) and Adobe Illustrator 24.2 (Adobe, Inc., San Jose, CA, USA). The correlations with $p \leq 0.05$ were considered significant. Where present, the row and column clustering of heatmaps was done using Euclidean distance and "ward.D" agglomeration method employed in *pheatmap* package in R.

Supplementary Materials: The following supporting information can be downloaded at: www.mdpi.com/xxx/s1, Figure S1: Raw images of membranes after chemiluminescent detection of target proteins and modifications.

Author Contributions: Conceptualization, V.I.B.; methodology, all the co-authors; resources, A.V.K., N.V.L., A.V.G. and V.I.B.; investigation, A.V.A., V.A.A., A.V.G., D.A.S., I.S.K, A.V.K.; validation, formal analysis, A.V.A., V.A.A., A.V.G. and V.I.B.; data curation, A.V.A., V.A.A., A.L.K., A.V.G.; writing—original draft preparation, A.V.A. and V.I.B.; writing—review and editing, V.I.B.; visualization, A.V.A., V.A.A. and V.I.B.; supervision, V.I.B.; project administration, V.I.B. and A.V.G.; funding acquisition, V.I.B and A.V.G. All authors have read and agreed to the published version of the manuscript.

Funding: This research was funded by Russian Foundation for Basic Research, grant number 20-54-7804 to A.V.G.

Institutional Review Board Statement: The animal study protocol was approved by the Bioethics Committee of Lomonosov Moscow State University (protocol numbers 69-o from 9 June 2016 and 139-a from 11.11.2021).

Data Availability Statement: Raw data are available from the authors upon request.

Conflicts of Interest: The authors declare no conflict of interest. The funders had no role in the design of the study; in the collection, analyses, or interpretation of data; in the writing of the manuscript, or in the decision to publish the results.

References

1. Bunik, V. Vitamin-dependent complexes of 2-oxo acid dehydrogenases: structure, function, regulation and medical implications; Nova Science Publishers: New York, 2017; pp. 203.
2. Choudhary, C.; Weinert, B.T.; Nishida, Y.; Verdin, E.; Mann, M. The growing landscape of lysine acetylation links metabolism and cell signalling. Nature reviews. Molecular cell biology **2014**, 15, 536-550, doi:10.1038/nrm3841.
3. Wagner, G.R.; Payne, R.M. Widespread and enzyme-independent Nepsilon-acetylation and Nepsilon-succinylation of proteins in the chemical conditions of the mitochondrial matrix. The Journal of biological chemistry **2013**, 288, 29036-29045, doi:10.1074/jbc.M113.486753.
4. Sutendra, G.; Kinnaird, A.; Dromparis, P.; Paulin, R.; Stenson, T.H.; Haromy, A.; Hashimoto, K.; Zhang, N.; Flaim, E.; Michelakis, E.D. A nuclear pyruvate dehydrogenase complex is important for the generation of acetyl-CoA and histone acetylation. Cell **2014**, 158, 84-97, doi:10.1016/j.cell.2014.04.046.
5. Hossain, A.J.; Islam, R.; Kim, J.G.; Dogsom, O.; Cap, K.C.; Park, J.B. Pyruvate Dehydrogenase A1 Phosphorylated by Insulin Associates with Pyruvate Kinase M2 and Induces LINC00273 through Histone Acetylation. Biomedicines **2022**, 10, doi:10.3390/biomedicines10061256.
6. Shi, Y.; Wang, Y.; Jiang, H.; Sun, X.; Xu, H.; Wei, X.; Wei, Y.; Xiao, G.; Song, Z.; Zhou, F. Mitochondrial dysfunction induces radioresistance in colorectal cancer by activating [Ca(2+)]m-PDP1-PDH-histone acetylation retrograde signaling. Cell death & disease **2021**, 12, 837, doi:10.1038/s41419-021-03984-2.
7. Aleshin, V.A.; Mkrtchyan, G.V.; Bunik, V.I. Mechanisms of Non-coenzyme Action of Thiamine: Protein Targets and Medical Significance. Biochemistry. Biokhimiia **2019**, 84, 829-850, doi:10.1134/S0006297919080017.
8. Bunik, V.I.; Aleshin, V.A. Analysis of the protein binding sites for thiamin and its derivatives to elucidate molecular mechanisms of the non-coenzyme action of thiamin (vitamin B1). Studies in Natural Products Chemistry **2017**, 53, 375-429.
9. Bunik, V.I.; Tylicki, A.; Lukashev, N.V. Thiamin diphosphate-dependent enzymes: from enzymology to metabolic regulation, drug design and disease models. The FEBS journal **2013**, 280, 6412-6442, doi:10.1111/febs.12512.
10. Bingham, P.M.; Stuart, S.D.; Zachar, Z. Lipoic acid and lipoic acid analogs in cancer metabolism and chemotherapy. Expert review of clinical pharmacology **2014**, 7, 837-846, doi:10.1586/17512433.2014.966816.
11. Stuart, S.D.; Schauble, A.; Gupta, S.; Kennedy, A.D.; Keppler, B.R.; Bingham, P.M.; Zachar, Z. A strategically designed small molecule attacks alpha-ketoglutarate dehydrogenase in tumor cells through a redox process. Cancer & metabolism **2014**, 2, 4, doi:10.1186/2049-3002-2-4.
12. Zachar, Z.; Marecek, J.; Maturo, C.; Gupta, S.; Stuart, S.D.; Howell, K.; Schauble, A.; Lem, J.; Piramzadian, A.; Karnik, S., et al. Non-redox-active lipoate derivates disrupt cancer cell mitochondrial metabolism and are potent anticancer agents in vivo. Journal of molecular medicine **2011**, 89, 1137-1148, doi:10.1007/s00109-011-0785-8.
13. Artiukhov, A.V.; Graf, A.V.; Bunik, V.I. Directed Regulation of Multienzyme Complexes of 2-Oxo Acid Dehydrogenases Using Phosphonate and Phosphinate Analogs of 2-Oxo Acids. Biochemistry. Biokhimiia **2016**, 81, 1498-1521, doi:10.1134/S0006297916120129.
14. Bunik, V.I.; Artiukhov, A.; Kazantsev, A.; Goncalves, R.; Daloso, D.; Oppermann, H.; Kulakovskaya, E.; Lukashev, N.; Fernie, A.; Brand, M., et al. Specific inhibition by synthetic analogs of pyruvate reveals that the pyruvate dehydrogenase reaction is essential for metabolism and viability of glioblastoma cells. Oncotarget **2015**, 6, 40036-40052, doi:10.18632/oncotarget.5486.

15. Aleshin, V.A.; Artiukhov, A.V.; Oppermann, H.; Kazantsev, A.V.; Lukashev, N.V.; Bunik, V.I. Mitochondrial Impairment May Increase Cellular NAD(P)H: Resazurin Oxidoreductase Activity, Perturbing the NAD(P)H-Based Viability Assays. Cells **2015**, 4, 427-451, doi:10.3390/cells4030427.
16. Tsepkova, P.M.; Artiukhov, A.V.; Boyko, A.I.; Aleshin, V.A.; Mkrtchyan, G.V.; Zvyagintseva, M.A.; Ryabov, S.I.; Ksenofontov, A.L.; Baratova, L.A.; Graf, A.V., et al. Thiamine Induces Long-Term Changes in Amino Acid Profiles and Activities of 2-Oxoglutarate and 2-Oxoadipate Dehydrogenases in Rat Brain. Biochemistry. Biokhimiia **2017**, 82, 723-736, doi:10.1134/S0006297917060098.
17. Graf, A.; Ksenofontov, A.; Bunik, V. Inhibition of 2-oxoglutarate dehydrogenase as a chemical model of acute hypobaric hypoxia. Frontiers in medicine **2021**, 8, 751639, doi:10.3389/fmed.2021.751639.
18. Nemeria, N.S.; Korotchkina, L.G.; Chakraborty, S.; Patel, M.S.; Jordan, F. Acetylphosphinate is the most potent mechanism-based substrate-like inhibitor of both the human and Escherichia coli pyruvate dehydrogenase components of the pyruvate dehydrogenase complex. Bioorganic chemistry **2006**, 34, 362-379, doi:10.1016/j.bioorg.2006.09.001.
19. Artiukhov, A.V.; Graf, A.V.; Kazantsev, A.V.; Boyko, A.I.; Aleshin, V.A.; Ksenofontov, A.L.; Bunik, V.I. Increasing Inhibition of the Rat Brain 2-Oxoglutarate Dehydrogenase Decreases Glutathione Redox State, Elevating Anxiety and Perturbing Stress Adaptation. Pharmaceuticals (Basel) **2022**, 15, doi:10.3390/ph15020182.
20. Bakovic, M.; Fullerton, M.D.; Michel, V. Metabolic and molecular aspects of ethanolamine phospholipid biosynthesis: the role of CTP:phosphoethanolamine cytidylyltransferase (Pcyt2). Biochem Cell Biol **2007**, 85, 283-300, doi:10.1139/o07-006.
21. Patel, D.; Witt, S.N. Ethanolamine and Phosphatidylethanolamine: Partners in Health and Disease. Oxid Med Cell Longev **2017**, 2017, 4829180, doi:10.1155/2017/4829180.
22. Jang, S.; Chapa-Dubocq, X.R.; Tyurina, Y.Y.; St Croix, C.M.; Kapralov, A.A.; Tyurin, V.A.; Bayir, H.; Kagan, V.E.; Javadov, S. Elucidating the contribution of mitochondrial glutathione to ferroptosis in cardiomyocytes. Redox biology **2021**, 45, 102021, doi:10.1016/j.redox.2021.102021.
23. Basu Ball, W.; Baker, C.D.; Neff, J.K.; Apfel, G.L.; Lagerborg, K.A.; Zun, G.; Petrovic, U.; Jain, M.; Gohil, V.M. Ethanolamine ameliorates mitochondrial dysfunction in cardiolipin-deficient yeast cells. The Journal of biological chemistry **2018**, 293, 10870-10883, doi:10.1074/jbc.RA118.004014.
24. Li, Y.; Lou, W.; Raja, V.; Denis, S.; Yu, W.; Schmidtke, M.W.; Reynolds, C.A.; Schlame, M.; Houtkooper, R.H.; Greenberg, M.L. Cardiolipin-induced activation of pyruvate dehydrogenase links mitochondrial lipid biosynthesis to TCA cycle function. The Journal of biological chemistry **2019**, 294, 11568-11578, doi:10.1074/jbc.RA119.009037.
25. Chu, C.T.; Ji, J.; Dagda, R.K.; Jiang, J.F.; Tyurina, Y.Y.; Kapralov, A.A.; Tyurin, V.A.; Yanamala, N.; Shrivastava, I.H.; Mohammadyani, D., et al. Cardiolipin externalization to the outer mitochondrial membrane acts as an elimination signal for mitophagy in neuronal cells. Nature cell biology **2013**, 15, 1197-1205, doi:10.1038/ncb2837.
26. Tucek, S. Problems in the organization and control of acetylcholine synthesis in brain neurons. Prog Biophys Mol Biol **1984**, 44, 1-46, doi:10.1016/0079-6107(84)90011-7.
27. Gibson, G.E.; Jope, R.; Blass, J.P. Decreased synthesis of acetylcholine accompanying impaired oxidation of pyruvic acid in rat brain minces. The Biochemical journal **1975**, 148, 17-23, doi:10.1042/bj1480017.
28. Gibson, G.E.; Ksiezak-Reding, H.; Sheu, K.F.; Mykytyn, V.; Blass, J.P. Correlation of enzymatic, metabolic, and behavioral deficits in thiamin deficiency and its reversal. Neurochemical research **1984**, 9, 803-814, doi:10.1007/BF00965667.
29. Gibson, G.; Barclay, L.; Blass, J. The role of the cholinergic system in thiamin deficiency. Annals of the New York Academy of Sciences **1982**, 378, 382-403, doi:10.1111/j.1749-6632.1982.tb31213.x.
30. Bizon-Zygmanska, D.; Jankowska-Kulawy, A.; Bielarczyk, H.; Pawelczyk, T.; Ronowska, A.; Marszall, M.; Szutowicz, A. Acetyl-CoA metabolism in amprolium-evoked thiamine pyrophosphate deficits in cholinergic SN56 neuroblastoma cells. Neurochemistry international **2011**, 59, 208-216, doi:10.1016/j.neuint.2011.04.018.
31. Jankowska-Kulawy, A.; Bielarczyk, H.; Pawelczyk, T.; Wroblewska, M.; Szutowicz, A. Acetyl-CoA and acetylcholine metabolism in nerve terminal compartment of thiamine deficient rat brain. Journal of neurochemistry **2010**, 115, 333-342, doi:10.1111/j.1471-4159.2010.06919.x.
32. Ronowska, A.; Gul-Hinc, S.; Michno, A.; Bizon-Zygmanska, D.; Zysk, M.; Bielarczyk, H.; Szutowicz, A.; Gapys, B.; Jankowska-Kulawy, A. Aggravated effects of coexisting marginal thiamine deficits and zinc excess on SN56 neuronal cells. Nutr Neurosci **2021**, 24, 432-442, doi:10.1080/1028415X.2019.1641296.
33. Hoshi, M.; Takashima, A.; Noguchi, K.; Murayama, M.; Sato, M.; Kondo, S.; Saitoh, Y.; Ishiguro, K.; Hoshino, T.; Imahori, K. Regulation of mitochondrial pyruvate dehydrogenase activity by tau protein kinase I/glycogen synthase kinase 3beta in brain. Proceedings of the National Academy of Sciences of the United States of America **1996**, 93, 2719-2723, doi:10.1073/pnas.93.7.2719.
34. Ronowska, A.; Dys, A.; Jankowska-Kulawy, A.; Klimaszewska-Lata, J.; Bielarczyk, H.; Romianowski, P.; Pawelczyk, T.; Szutowicz, A. Short-term effects of zinc on acetylcholine metabolism and viability of SN56 cholinergic neuroblastoma cells. Neurochemistry international **2010**, 56, 143-151, doi:10.1016/j.neuint.2009.09.012.
35. Baillie, A.C.; Wright, K.; Wright, B.J.; Earnshaw, C.G. Inhibitors of pyruvate dehydrogenase as herbicides. Pesticide Biochemistry and Physiology **1988**, 30, 103-112, doi:10.1016/0048-3575(88)90044-2.
36. Kim, M.J.; Hennen, W.J.; Sweers, H.M.; Wong, C.H. Enzymes in carbohydrate synthesis: N-acetylneuraminic acid aldolase catalyzed reactions and preparation of N-acetyl-2-deoxy-D-neuraminic acid derivatives. Journal of the American Chemical Society **1988**, 110, 6481–6486, doi:10.1021/ja00227a031.

Preprints (www.preprints.org) | NOT PEER-REVIEWED | Posted: 3 October 2022 doi:10.20944/preprints202210.0006.v1

37. Aleshin, V.A.; Graf, A.V.; Artiukhov, A.V.; Boyko, A.I.; Ksenofontov, A.L.; Maslova, M.V.; Nogues, I.; di Salvo, M.L.; Bunik, V.I. Physiological and Biochemical Markers of the Sex-Specific Sensitivity to Epileptogenic Factors, Delayed Consequences of Seizures and Their Response to Vitamins B1 and B6 in a Rat Model. Pharmaceuticals (Basel) **2021**, 14, doi:10.3390/ph14080737.
38. Aleshin, V.A.; Mkrtchyan, G.V.; Kaehne, T.; Graf, A.V.; Maslova, M.V.; Bunik, V.I. Diurnal regulation of the function of the rat brain glutamate dehydrogenase by acetylation and its dependence on thiamine administration. Journal of neurochemistry **2020**, 153, 80-102, doi:10.1111/jnc.14951.
39. Graf, A.V.; Maslova, M.V.; Artiukhov, A.V.; Ksenofontov, A.L.; Aleshin, V.A.; Bunik, V.I. Acute prenatal hypoxia in rats affects physiology and brain metabolism in the offspring, dependent on sex and gestational age. International journal of molecular sciences **2022**, 23, 2579, doi:10.3390/ijms23052579.
40. Ksenofontov, A.L.; Boyko, A.I.; Mkrtchyan, G.V.; Tashlitsky, V.N.; Timofeeva, A.V.; Graf, A.V.; Bunik, V.I.; Baratova, L.A. Analysis of Free Amino Acids in Mammalian Brain Extracts. Biochemistry. Biokhimiia **2017**, 82, 1183-1192, doi:10.1134/S000629791710011X.
41. Artiukhov, A.V.; Grabarska, A.; Gumbarewicz, E.; Aleshin, V.A.; Kahne, T.; Obata, T.; Kazantsev, A.V.; Lukashev, N.V.; Stepulak, A.; Fernie, A.R., et al. Synthetic analogues of 2-oxo acids discriminate metabolic contribution of the 2-oxoglutarate and 2-oxoadipate dehydrogenases in mammalian cells and tissues. Scientific reports **2020**, 10, 1886, doi:10.1038/s41598-020-58701-4.
42. Ladner, C.L.; Yang, J.; Turner, R.J.; Edwards, R.A. Visible fluorescent detection of proteins in polyacrylamide gels without staining. Analytical biochemistry **2004**, 326, 13-20, doi:10.1016/j.ab.2003.10.047.